Version of Record: https://www.sciencedirect.com/science/article/pii/S0011227518300328
Manuscript_be66d331f11e3232170a418a3801943c

# TITLE

Forced Flow Cooling of High Field, REBCO-Based, Fusion Magnets Using Supercritical Hydrogen, Helium, and Neon

# AUTHORS

Julien Barber [a,b], John Brisson [a,c], Joseph Minervini [a,d]

[a] Plasma Science and Fusion Center
Department of Mechanical Engineering
Massachusetts Institute of Technology
NW16, 167 Albany St.
Cambridge, MA 02139

[b] jbarber@mit.edu
[c] brisson@mit.edu
[d] minervini@psfc.mit.edu

Corresponding Author: Julien Barber
**Email:** jbarber@mit.edu

© 2018 published by Elsevier. This manuscript is made available under the Elsevier user license
https://www.elsevier.com/open-access/userlicense/1.0/

# ABSTRACT

Rare Earth Barium Copper Oxide (REBCO)[1] High Temperature Superconductor (HTS) tapes are being considered for the Toroidal Field (TF) magnets of a highly compact, high field fusion reactor operating at magnetic fields as high as 21 T and operating temperatures in the range of 10-30 K. Due to the increase in range of operating conditions made available through HTS tapes, a new set of cryogenic fluids are being considered for forced flow cooling. The present study investigates helium, hydrogen, and neon as a forced flow coolant for REBCO HTS tapes used in a highly compact, high-field reactor design. Four design criteria are considered, including current sharing temperature, fluid inlet temperature, cable pressure drop (dP), and operating pressure. From these simulations, neon is removed from consideration due to its high required pressure drop and low temperature margins with respect to the current sharing limit. Helium and hydrogen are then compared, with hydrogen producing the highest overall heat transfer rate at its optimum operating condition (1.5 MPa/ 15 K). A compromise across inlet temperature, dP, and operating pressure is found when helium has a minimum initial temperature of 10 K and an inlet pressure of 2.0 MPa. For the current design, helium is selected as a coolant due its acceptable cable pressure drop, required cooling load, and system complexity inherent to a forced-flow cryogenic system.

**Key Words:** Forced-flow cooling, high-temperature superconductors, fusion, magnets, supercritical fluid, high heat flux, heat transfer, REBCO

# 1.0 INTRODUCTION

In a tokamak fusion system, the available fusion power is proportional to the magnetic field to the fourth power [1]. Consequently, a new generation of fusion reactors are under development, utilizing a high field approach to produce power [1-4]. The advent of high-field tokamaks has been in large part due to the recent development of high-temperature superconductors (HTS)[2]. Use of HTS tape in tokamak magnet systems provides the ability to transfer the required coil current with zero resistive losses. However, what distinguishes HTS from its low-temperature counterparts, is its ability to maintain high critical current densities at elevated temperatures and magnetic fields. In doing so, HTS achieves increased thermal stability to protect against magnet system failure, and allows operation at temperatures high enough for tokamak designs to reduce the thickness of the nuclear radiation shield; thereby reducing the overall size and cost of the machine.

Reducing size, cost, and complexity of fusion machines presents an ideal pathway for tokamak design [1]. However, reducing the nuclear radiation shield results in an increase in thermal loads to the magnets due to neutron loading. Within every tokamak magnet, the cryogen must be able to remove these highly variable thermal loads from the nuclear reaction, heat from AC losses, current leads, as well as eddy currents induced within the magnets themselves. In a low-shielding tokamak, the neutron thermal loads are vastly dominant.

Prior superconducting materials have required operation within 2-4 K, thereby limiting the cryogen selection to helium, and the heat transfer potential to the associated thermal-fluid properties. High nuclear heat loads present a challenge for forced-flow helium cooling due to helium's limited heat capacity and density. The high operating temperature associated with HTS material opens new opportunities to explore different cryogens as working fluids for fusion magnet systems. Hydrogen and neon now present themselves as possible improved working fluids due to their high thermal conductivity, density, specific heat, and low viscosity. The current paper explores the use of these cryogens as a forced flow coolant for REBCO HTS tapes used in the toroidal field (TF)[3] magnets of a highly compact, high-field reactor design. A thermal-fluid analysis is conducted which investigates the intrinsic behavior of each cryogen as a potential coolant, and a numerical model is constructed to determine the necessary flow conditions to achieve safe thermal operation of a generic TF magnet.

[1] Rare Earth Barium Copper Oxide (REBCO)
[2] High-Temperature Superconductors (HTS)
[3] Toroidal Field (TF)

# 2.0 DESIGN METHODOLOGY

Within a TF coil, conductors are wound in a pancake configuration, and stacked in the toroidal direction. To assess the effectiveness of each cryogen as a coolant, a thermal-fluid analysis is applied to a single, unwound TF conductor. In this analysis, it is assumed that the coolant in each conductor cooling channel is capable of removing the volumetric heat deposited in the surrounding solid material (i.e. each cable is thermally isolated from one another). In the current study, an arbitrary design is chosen to represent a feasible representation of a high-field TF coil (Fig.1).

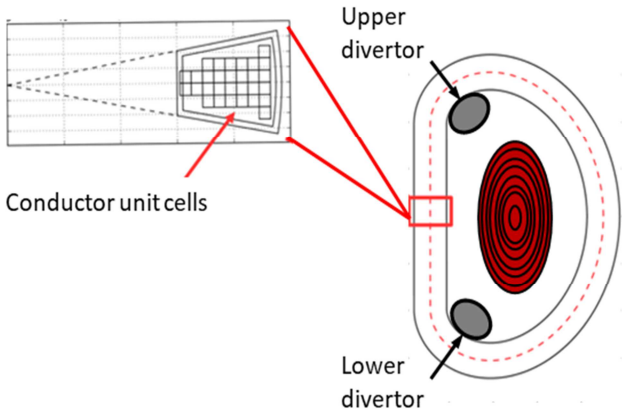


Figure 1- Internal cable winding configuration of TF coil

The proposed cable design relates to a 100-m long conductor (representing the unwound length of one possible TF cable) using the conductor geometry shown in Fig. 2. The working fluid flows through the inner cylindrical channel, while the neutrons heat the copper/HTS matrix and steel structure volumetrically. For the purposes of this paper, the flow length is 50-m from the inlet at the center of the cable length with two outlets at opposite ends, representing flow through a double pancake winding geometry. Furthermore, despite the high potential heat transfer associated with two-phase flow, the fluid in the present study is restricted to the single-phase regime to avoid potential dry-out resulting in magnet system failure.

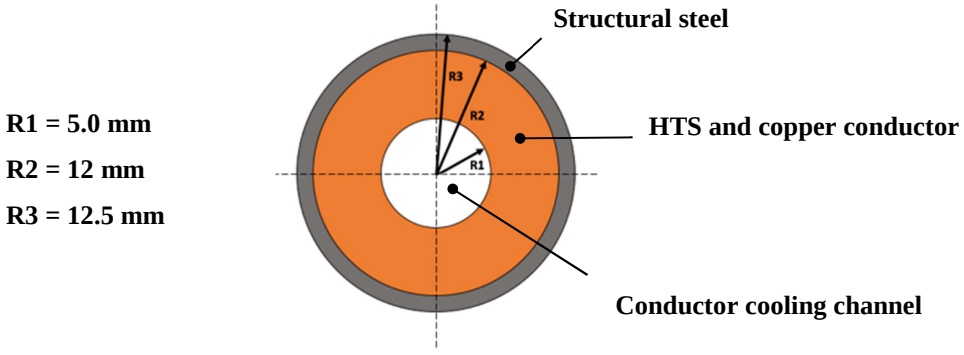


Figure 2 - Cross section of cable geometry (conductor unit cell)

Using Direct Accelerated Geometry Monte Carlo (DAGMC) software and a Monte Carlo N-Particle (MCNP5) neutron transport code, the neutron heating profile along a single unwound cable length was estimated for a specific geometry and plasma operation (Fig.3). Each set of three peaks represents one turn in the TF coil. The bounding peaks in each set of three result from a low shielding thickness near the upper and lower divertor regions, while the central peak is a result of the heat deposited at the mid plane of the plasma. As the conductor is wound radially outwards, the volumetric heat flux decays exponentially as the neutrons pass through solid material and lose energy.

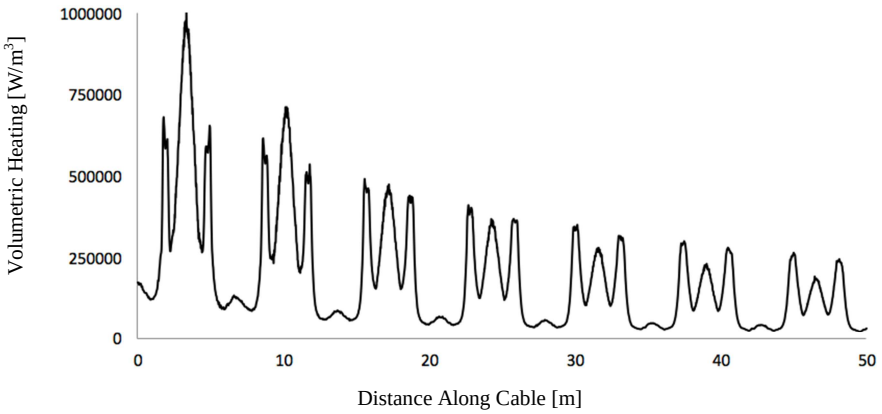


Figure 3 –Assumed volumetric nuclear heating profile along a single TF cable length

The present design assumes that the plasma is pulsed for ten seconds. During this time, the cryogen is required to limit the temperature of the conductor below the current sharing temperature, defined as the point which the superconducting cable becomes resistive and Joule heating occurs. The current sharing temperature is a local function of the critical current density and maximum magnetic field on the conductor. For the current study, the maximum field on coil is assumed to be 21 T and the operating current density is defined at 637 A/mm$^2$ [4]. With a given field strength and operating current density, the current sharing temperature can be defined on the critical surface of the REBCO HTS tape.

Every superconducting material operates at a temperature under the current sharing limit defined by the material's critical surface. Compared to LTS, HTS provides nearly a 10x improvement in the critical surface, drastically increasing the potential operating range of the superconducting material (Fig. 4). The enhanced operating envelope of HTS is what allows consideration of cryogenic fluids other than helium for cooling the magnet systems.

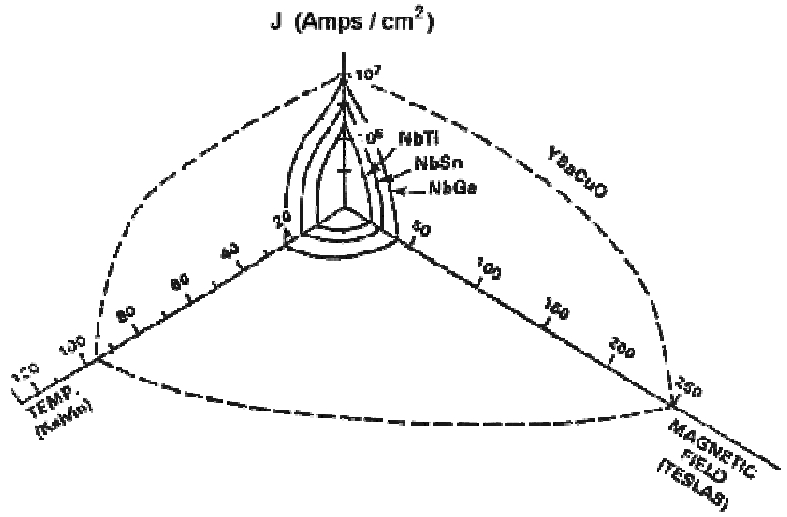


Figure 4 - Critical surface of HTS and LTS as a function of temperature and magnetic field

Fig.5 shows the current sharing temperature for the REBCO tape used in the base case design. The steps in the temperature limit are due to the decay of the magnetic field in the radial direction. As the magnetic field decays, at constant current density, the current sharing temperature increases proportionally. The current sharing temperature provides insights into the maximum allowable temperature rise for each cryogen. For example, since hydrogen must operate above 15 K to avoid solidification, the maximum allowable temperature rise in the first cable turn corresponds to approximately 15 K. The current sharing data will be used to help assess each cryogen based on their fluid properties and will be used in the numerical model as a required design criteria.

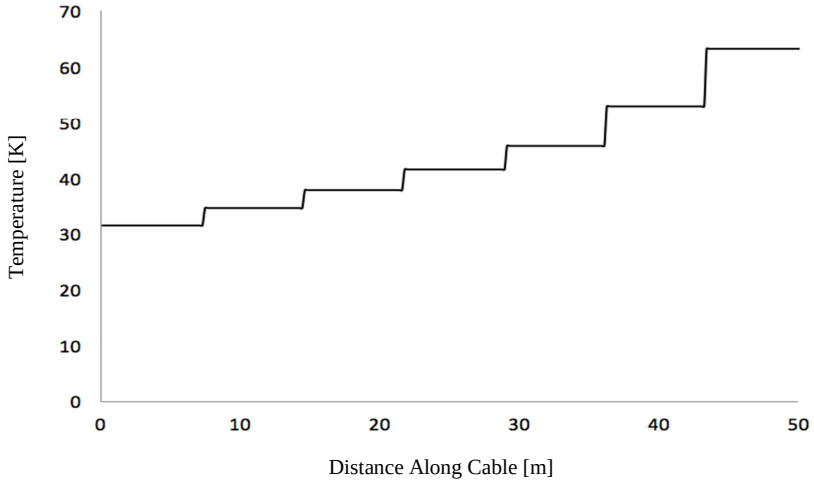


Figure 5 - Cable current sharing temperature for a maximum field strength of 21 T and conductor temperature of 20 K

# 3.0 CRYOGEN ASSESSMENT

Prior to the numerical analysis of the TF cable, an assessment of the thermo-fluid properties of each cryogen is conducted to determine the potential for heat transfer. The heat transfer potential is evaluated in terms of volumetric heat capacity and heat transfer coefficient (HTC) as they relate to a baseline cable model (outlined in Section 2.0) for supercritical helium, hydrogen, and neon. Each fluid has significantly different properties governed by their atomic structure and intermolecular interactions. Fig. 6 illustrates the temperature-entropy diagram for helium, hydrogen, and neon from 0.5- 3.5 MPa. There are three sets of curves shown that correspond to each of the three considered cryogens. Each of these sets constitute a plot of the saturated states and a set of isobars that span from 0.5 MPa to 3.5 MPa.

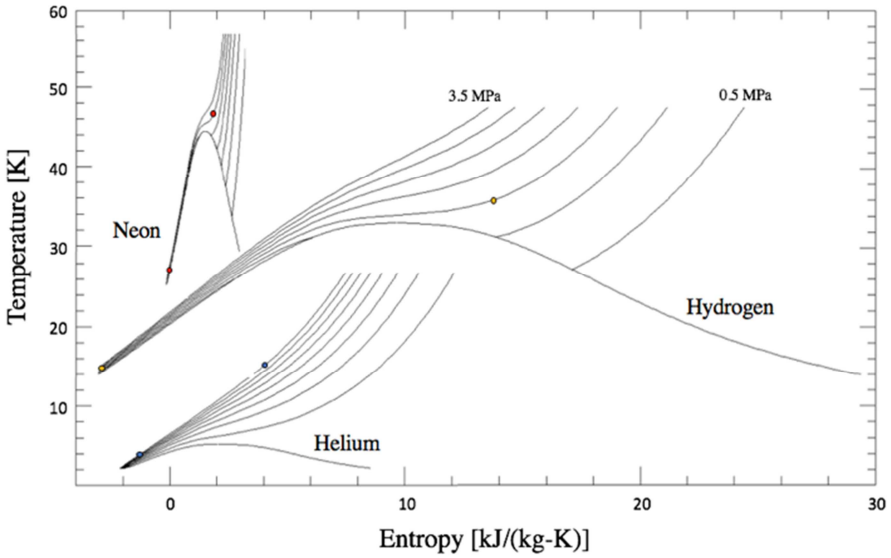


Figure 6 - Temperature-entropy plot for helium, hydrogen, and neon with isobars from 0.5-3.5 MPa accompanied by a summary of critical state points for each fluid.

The T-s diagram visualizes the operating regions and relative heat capacity for each fluid. Typically, the specific heat of a fluid is representative of its ability to absorb energy and regulate temperature. However, we are interested in the fluid's ability to absorb energy in a forced flow scenario. Therefore, to make an accurate comparison between cryogens it is necessary to compare the energy absorption potential on a unit volume basis. Fig. 7 shows the volumetric heat capacity of single-phase helium, hydrogen, and neon as a function of temperature and pressure.

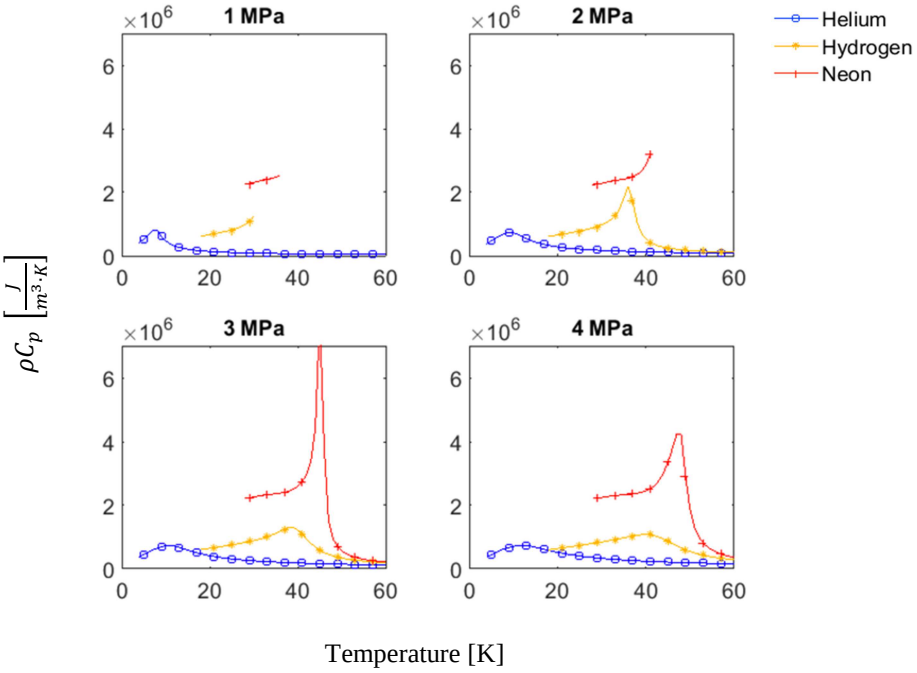


Figure 7 – Single phase volumetric heat capacity at constant pressures (1-4 MPa) and varying temperature.

Neon and hydrogen show limited data since Fig. 7 shows only the single phase $\rho C_p$ for the three fluids. For the single-phase regions considered, neon provides a consistently higher volumetric heat capacity compared to hydrogen and helium ranging from 160-610% and 320-1070% respectively. Moreover, it is clear from Fig. 7 that each fluid has a specific range of temperatures associated with its peak storage capacity. For example, helium is most effective from 5-10 K, while hydrogen and neon perform best at 20-30 K and 30-40 K respectively. These optimum temperatures correspond to the critical point of the fluid, and increase in range as pressure rises.

Neon possesses a higher volumetric heat capacity at a constant inlet pressure when compared to helium and hydrogen. However, when assessing a cryogen's heat transfer potential in a forced flow scenario, the volumetric heat capacity is only one of the relevant fluid properties. The HTC is the quantitative measure that describes the effectiveness of heat transfer between two media. In the present study, we are interested in comparing the HTC for common pressure drops (dP), since the effective dP across the cable is a critical design criteria for pump sizing and cable design. In the analysis of each fluid, the cable geometry, length, and material are fixed according to the design outlined in Section 2.0. By varying dP, the velocity of each fluid is calculated and used in the Dittus-Boelter correlation to estimate the overall HTC [5]. Fig. 8 shows the resulting heat transfer coefficients for each fluid at varying dP and for fluid properties at a constant initial pressure of 3.0 MPa. By fixing the operating pressure at 3.0 MPa, each fluid remains supercritical (single phase), and a standardized comparison can be made.

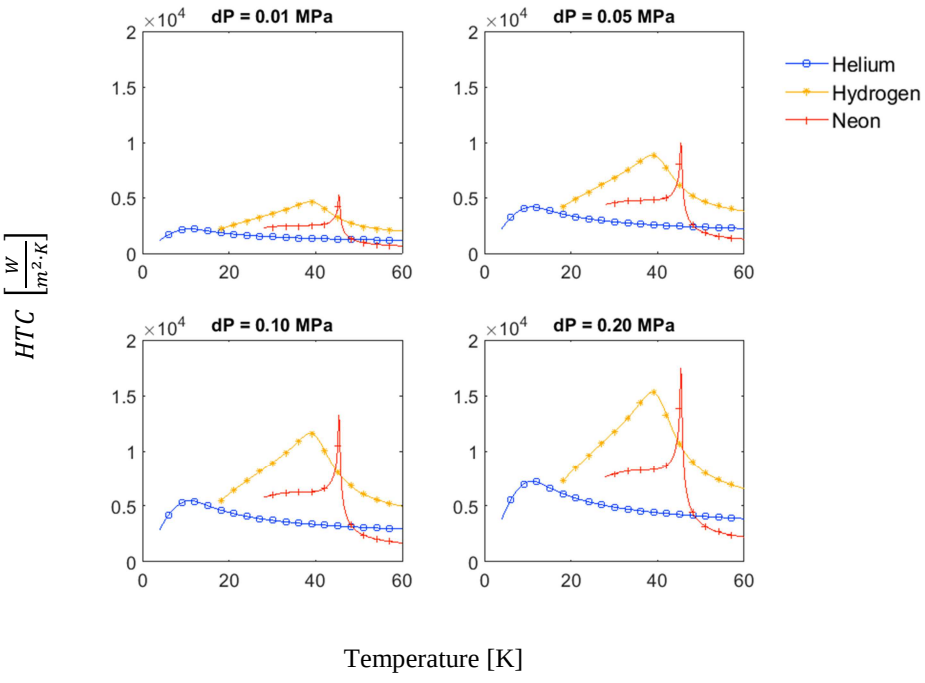


Figure 8 - Heat transfer coefficient (Dittus-Boelter) at a constant pressure of 3.0 MPa, with cable pressure drop varying from 0.01-0.20 MPa - reference cable geometry.

Similar to the volumetric heat capacity, Fig. 8 identifies an optimum operating temperature range for each fluid, recognized as the range of increasing HTC. However, in contrast to the volumetric heat capacity, hydrogen now produces higher heat transfer rates when compared to both helium and neon. The reason for hydrogen's high cooling potential can be determined through analyzing the Dittus-Boelter correlation in greater detail. Assuming each cryogen behaves classically, the heat transfer coefficient can be found to be proportional to: $h \propto (\rho C_p)^{0.4} \cdot (k)^{0.6} \cdot (\mu)^{-0.4}$

Table 1 shows the comparative increase in neon's properties compared to helium and hydrogen at an operating point of 30 K and 3.0 MPa. Neon has a viscosity that is over 1000% greater than hydrogen, with a volumetric heat capacity and thermal conductivity of only 150% and 37% larger, respectively. As compared to hydrogen, neon's increase in viscosity far outweighs the effects on HTC due to differences in volumetric heat capacity and thermal conductivity. Since viscosity is inversely proportional to the HTC, this results in a net decrease in HTC.

Table 1 – Key HTC properties of neon, hydrogen, and helium.

| | $\rho C_p \left[10^5 \cdot \frac{J}{m^3 K}\right]$ | $k \left[10 \cdot \frac{W}{mK}\right]$ | $\mu$ [$10^{-6}$ ·Pa s] |
|---|---|---|---|
| Neon | 22.50 | 1.44 | 95.6 |
| Hydrogen | 8.89 | 1.06 | 8.73 |
| Helium | 2.54 | 0.41 | 5.40 |

Fig. 9 shows the variation in HTC with respect to temperature for lines of constant pressure. Each graph is plotted for a constant dP = 0.20 MPa, and over a temperature range wide enough to show the entire profile - limited at the lower limit by the fluid's solidification temperature.

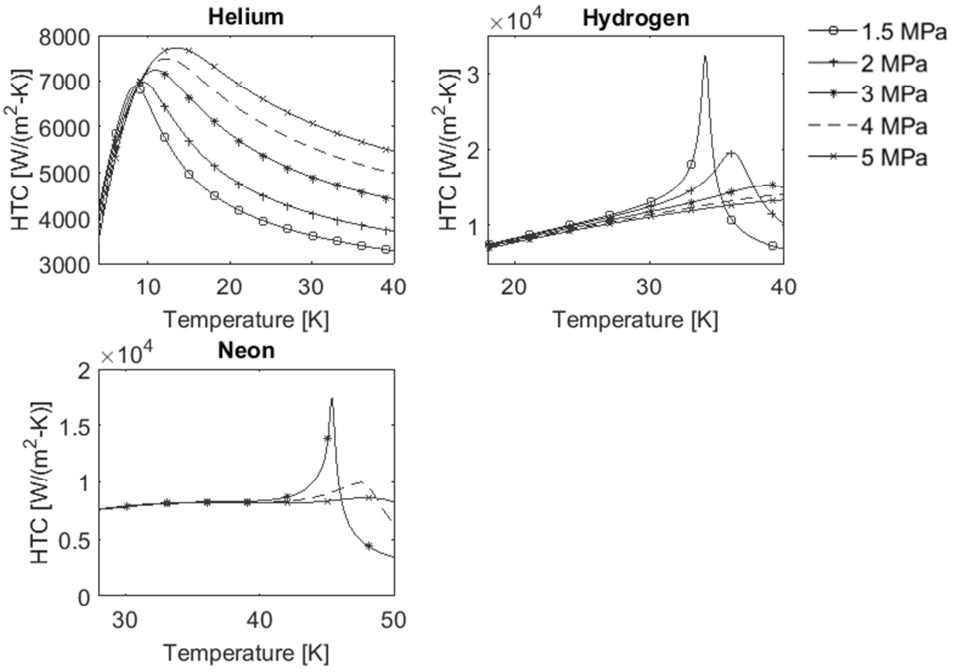


Figure 9 - Variation in HTC with respect to temperature for a series of constant pressures and a cable pressure drop of 0.20 MPa - reference cable geometry.

For helium, the HTC steadily rises with increasing pressure since the operating conditions are well into the supercritical region where the fluid behaves much like a gas. Conversely, hydrogen and neon have specific peak pressures associated with their critical point. At 1.5 MPa, the HTC of hydrogen reaches a maximum across the 15-40 K specified temperature range. Similarly, neon reaches a maximum HTC around 3.0 MPa across its temperature range of 27-50 K. Fig. 10 shows the maximum HTC on a given isobar for temperatures between 4-60 K, plotted as a function of pressures, and for mass flow corresponding to pressure drop from 0.01-0.20 MPa. Once more, there is a steady rise in the maximum HTC of helium with pressure, as well as a peak HTC for hydrogen, just below 1.5 MPa, and for neon, just below 3.0 MPa.

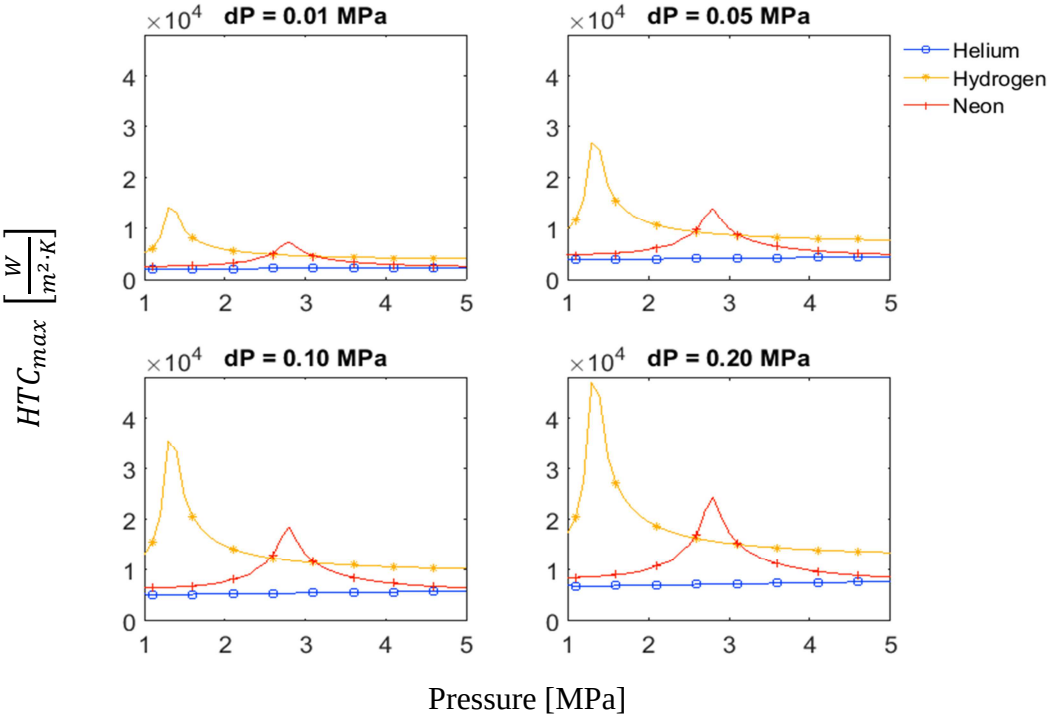


Figure 10 - Maximum HTC for a temperature range from 4-60K, as a function of pressure (1-5 MPa), and for constant pressure drops relating to the reference cable geometry.

Using the thermophysical properties of helium, hydrogen, and neon, the HTC is calculated for varying cable pressure drops using the Dittus-Boelter correlation. From this, an "optimum" initial operating condition can be determined for each fluid. The selected temperatures are identified as the range of increasing HTC that were found through the analysis in Fig. 8. Similarly, the optimum operating pressure (in parentheses next to each fluid label) is established through insights gained from Fig. 9 and Fig. 10. Table 2 summarizes these optimum conditions and displays the average expected heat transfer coefficients for each cryogen at a cable pressure drop of 0.20 MPa. The mean HTC at each fluid's optimum condition is displayed to provide a quantitative comparison across the three fluids for similar flow conditions. To define the average HTC, the arithmetic mean is calculated at the optimum fluid pressure for 0.01 K temperature steps along the optimum operating temperature range for a flow rate corresponding to dP = 0.20 MPa.

Table 2 - Summary of heat transfer characteristics for considered cryogens

| ***dP = 0.20 MPa*** | **Helium (3.5 MPa)** | **Hydrogen (1.5 MPa)** | **Neon (3.0 MPa)** |
|---|---|---|---|
| Optimum Operating Temperatures [K] | 5-15 | 15-35 | 27-46 |
| Peak Heat Transfer Coefficient [$W/(m^2K)$] | 7,370 | 32,330 | 17,450 |
| Mean Heat Transfer Coefficient Over Optimum Temperature Range [$W/(m^2K)$] | 6,510 | 12,410 | 8,110 |
| Normalized Cost [compared to He] | 1.0 | 0.2 | 58.0 |
| Gas Classification | Inert | Flammable | Inert |

In the case of a fusion device, large pressure drops and temperature variations occur within the superconducting cables due to the forced flow in the cable and the neutron heat load – a factor neglected in the current assessment. Therefore, significant property variations occur along the cable length, resulting in changes to the HTC. Accordingly, the heat transfer between the solid-fluid interface requires the use of a more complex model in order to accurately identify a working fluid for the current application.

# 4.0 THEORY

To investigate each cryogen for use in a TF magnet, a model is constructed that solves the energy equations for both the solid and fluid interfaces using a numerical approximation for a set of second order differential equations. To make use of the governing equations and numerical methods used in this paper, the following assumptions are made:

1. Fluid properties remain constant in each differential element - interpolated from the NIST REFPROP database for each fluid [6]
2. Cryogen behaves as a Newtonian fluid
3. The outer surface of the cable is adiabatic
4. Viscous heating/dissipation is negligible compared to neutron heating
5. No radiative heat transfer
6. Direct volumetric neutron heating of the cryogen is negligible
7. Fluid flow is unidirectional in the axial direction

## 4.1 Governing Equations

The continuity equations of mass, momentum, and energy form the foundation for which the model is constructed. With the assumption that the geometry is axisymmetric and the flow in purely axial, the three continuity equations can be converted to the form used in the current model. Assuming fully developed flow, mass conservation states:

$$\frac{\partial \dot{m}}{\partial x} = -A\frac{\partial \rho}{\partial t} \qquad \text{[Eq.1]}$$

Momentum conservation can similarly be manipulated to show that:

$$\frac{\partial P}{\partial x} = -\frac{1}{A^2}\left(\frac{\partial\left(\dot{m}^2/\rho\right)}{\partial x}\right) - \frac{1}{A}\left(\frac{\partial \dot{m}}{\partial t}\right) - \frac{f}{2D}\frac{\dot{m}^2}{A^2\rho} \qquad \text{[Eq.2]}$$

Eq. 2 simplifies to the familiar Darcy–Weisbach equation for pressure drop in a cylindrical pipe with uniform diameter when the mass flow rate derivatives go to zero. In Eq.2, $f$ is calculated using the transcendental Colebrook expression [7], which is valid for a wide range of flow conditions.

$$\frac{1}{\sqrt{f}} = -2\log\left[\frac{e/D}{3.7} + \frac{2.51}{Re_D\sqrt{f}}\right] \qquad \text{[Eq.3]}$$

Next, the energy equation can be reduced to the thermal equation given by:

$$\rho C_p \left[\frac{\partial T}{\partial t} + v\frac{\partial T}{\partial x}\right] = k\left(\frac{\partial^2 T}{\partial x^2} + \frac{1}{r}\frac{\partial}{\partial r}\left(r\frac{\partial T}{\partial r}\right)\right) + \dot{Q}_v + \mu\Phi \quad \text{[Eq.4]}$$

Within Eq.4, the viscous heating $\mu\Phi$ in the fluid interface is small compared to the magnitude of neutron heating $\dot{Q}_v$, and is thus neglected. Therefore, the governing thermal equations for the solid (Eq.5 and subscript 's') and fluid (Eq.6 and subscript 'f') interfaces are modeled as:

$$\rho C_p \left[\frac{\partial T_s}{\partial t}\right] = -k\left(\frac{\partial^2 T_s}{\partial x^2} + \frac{1}{r}\frac{\partial}{\partial r}\left(r\frac{\partial T_s}{\partial r}\right)\right) + \dot{Q}_{nuc} \quad \text{[Eq.5]}$$

$$\rho C_p \left[\frac{\partial T_f}{\partial t} + u\frac{\partial T_f}{\partial x}\right] = -k\left(\frac{\partial^2 T_f}{\partial x^2} + \frac{1}{r}\frac{\partial}{\partial r}\left(r\frac{\partial T_f}{\partial r}\right)\right) \quad \text{[Eq.6]}$$

The term $\dot{Q}_{nuc}$ does not appear in Eq.6 since the neutrons effectively pass through the cryogen without depositing substantial thermal energy within the fluid. In addition to the set of assumptions outlined in the formulation of Eq.1-Eq.6, the assumption of Newtonian fluid mechanics allows us to linearize the viscous stresses arising from the flow in proportion to the local strain rate. Doing so allows simplification of the thermal energy equation from the total energy equation.

An implicit Gauss-Seidel iteration calculates the solution to Eq.5 and Eq.6 to a convergence tolerance of 0.001%. Transient behavior is included with an upper limit time step of 0.3 seconds for each iteration - selected to maintain accuracy and minimize solution run time. The geometric mesh is spaced in the radial and axial directions, with the governing equations solved at each node. At each increment in time and position, the properties are evaluated using data from the National Institute of Standards and Technology's REFPROP [6] and the Copper Development Association's material property database [8].

## 4.2 Initial and Boundary Conditions

Equations 5 and 6 are second order in space, and therefore require two boundary conditions in both the radial and axial directions for each of the solid and fluid domains. Additionally, one initial condition is required to satisfy the first order transient term in both Eq. 5 and Eq. 6. For this paper, it is assumed that thermal equilibrium is reached between the fluid and solid domains prior to initializing the neutron heat source. Consequently, the initial conditions for both solid ('s') and fluid ('f') domains are given as:

$$T_{s,i} = T_{f,i} = T_i \quad \text{[Eq.7]}$$

where the subscript 'i' indicates the initial condition at t = 0.

### 4.2.1 Radial Boundary Conditions

Boundary conditions are used at r = 0 and r = $R_3$ (Fig.2), as well as the heat transfer at the fluid-copper ($R_1$) and copper-steel interfaces ($R_2$). At r = 0 and r = $R_3$, symmetry and the adiabatic cable condition implies that:

$$\left.\frac{\partial T_f}{\partial r}\right|_{r=0} = \left.\frac{\partial T_s}{\partial r}\right|_{r=R_3} = 0 \qquad \text{[Eq.8]}$$

Next, an energy balance at the fluid-copper interface demands that:

$$h\left(T_s - T_f\right) = -k_{CU}\left.\frac{\partial T_s}{\partial r}\right|_{r=R_1} \qquad \text{[Eq.9]}$$

In Eq.9, $T_f$ represents the bulk temperature of the fluid. Furthermore, the heat transfer coefficient is found using the updated Gnielinkski correlation [9], which reduces errors from the Dittus-Boelter correlation for flow in smooth pipes from 25% to less than 10%. The Gnielinski correlation is valid for $0.5 \leq Pr \leq 2000$ and $3000 \leq Re_D \leq 5 \times 10^6$, with the friction factor $f$ calculated using the relation given in Eq. 3.

$$Nu_D = \frac{(f/8)(Re_D - 1000)Pr}{1 + 12.7(f/8)^{1/2}(Pr^{2/3} - 1)} = \frac{h(2R_1)}{k_f} \qquad \text{[Eq.10]}$$

Finally, assuming negligible contact resistance, an energy balance at the copper-steel interface provides the fourth boundary condition r = $R_2$ as:

$$k_{CU}\left.\frac{\partial T_s}{\partial r}\right|_{r=R_2} = k_{ST}\left.\frac{\partial T_s}{\partial r}\right|_{r=R_2} \qquad \text{[Eq.11]}$$

### 4.2.2 Axial Boundary Conditions

In addition to the radial conditions, four boundary conditions are required to satisfy the second order differential equations with respect to the axial direction for both the solid and fluid domains. For the solid interface the adiabatic cable condition at x = 0 and x = L implies that:

$$\left.\frac{\partial T_s}{\partial x}\right|_{x=0} = \left.\frac{\partial T_s}{\partial x}\right|_{x=L} = 0 \qquad \text{[Eq.12]}$$

The third boundary condition for the fluid interface is determined by the constant inlet temperature to the test sample.

$$T_f\big|_{x=0} = T_{inlet} \qquad \text{[Eq.13]}$$

Finally, the fourth boundary condition is associated with the flow condition at the cable outlet. The model assumes that the only heat transfer occurring across the boundary is due to convection, resulting in:

$$\left.\frac{\partial^2 T_f}{\partial x^2}\right|_{x=L} = 0 \qquad \text{[Eq.14]}$$

For every node in the system, Eq. 5 and Eq. 6 are solved using the eight boundary conditions and two initial conditions outlined above. Using this model, the HTC can be solved along the entire length of the cable, and be used to determine the required operating conditions to achieve the current sharing limit.

# 5.0 RESULTS

Through the analysis in Section 3.0, an optimal range of operating conditions are identified. Through this assessment, a set of optimum initial conditions for each fluid are identified (Table 3). In each case, the initial conditions represent the expected peak performance of the fluid. The current analysis begins with comparing each fluid at these optimum conditions, then investigates the quantitative trade-offs associated with each fluid, only considering operating parameters that ensures the fluid remains single phase.

Table 3 - Summary of initial operating conditions for helium, hydrogen, and neon

| | Helium | Hydrogen | Neon |
|---|---|---|---|
| Temperature [K] | 5 | 15 | 30 |
| Pressure [K] | 3.5 | 1.5 | 3.0 |

Using the 2D model described in Section 4.0, the HTC for each cryogen is calculated given the optimum initial conditions outlined in Table 3, and for the tokamak design outlined in Section 2.0 (Fig. 11).

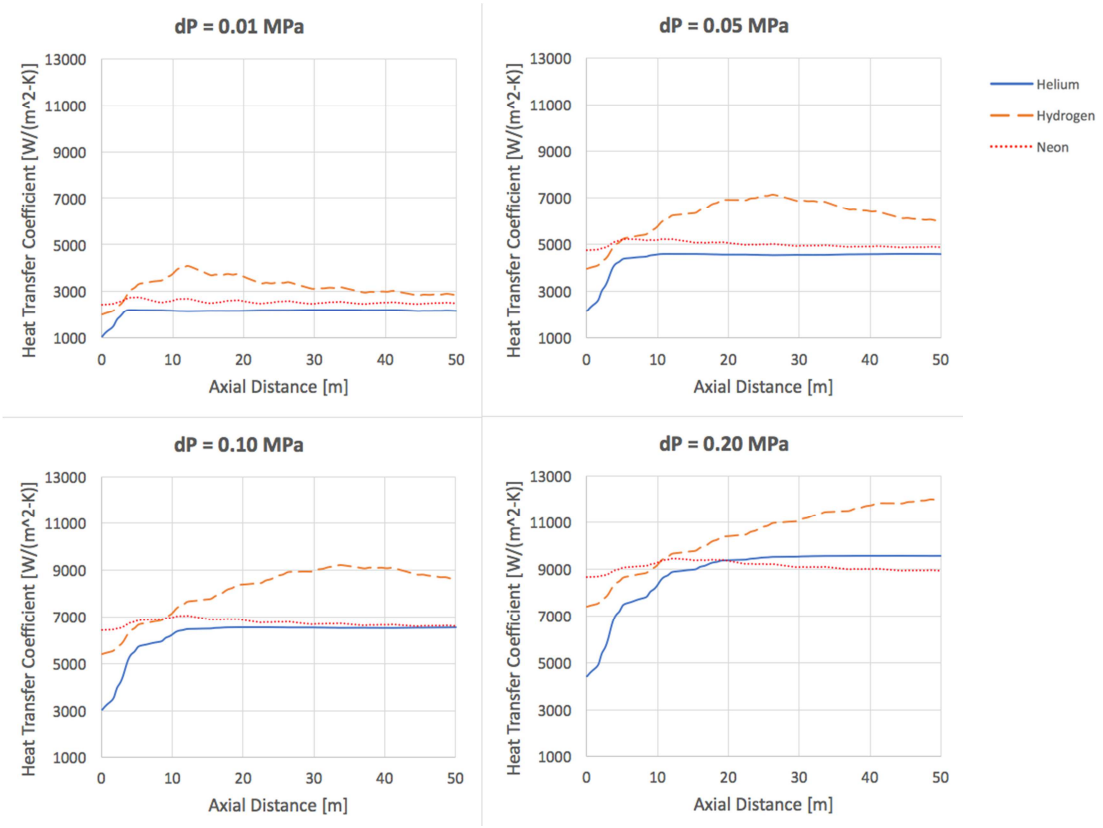


Figure 11 - HTC along the axial length of the cable for helium, hydrogen, and neon. The HTC is calculated at the optimum operating conditions (*) in Table 3

Consistent with the previous cryogen assessment, hydrogen can be classified as the most effective cryogen from the perspective of heat transfer. However, the HTC is not the only measure to be considered in the design of a TF coil. Ultimately, each cryogen must be able to limit the temperature rise of the conductor under the required current sharing temperature limit. To remain under the current sharing limit, trade-offs exist between three different operating parameters: (1) inlet fluid temperature, (2) pressure drop, and (3) operating pressure. The inlet temperature of the cryogen relates to the required refrigeration capacity since refrigeration efficiencies decrease exponentially at low temperatures. The pressure drop is across the cable length, and the operating pressure relates to the initial pressure of each fluid. Ultimately, cryogen selection comes down to a compromise across these factors.

To explore the trade-offs for each fluid, the three operating parameters are varied to ensure the current sharing requirement is met. Fig. 12 shows the conductor temperature profiles for each cryogen operating at the optimum initial pressures and temperatures outlined in Table 3. All three of the fluids engage with the current sharing limit at the first cable turn. However, the operating parameters required for the fluids to achieve the current sharing condition vary. For example, the required pressure drop for neon at optimum conditions is 37 times greater than for helium and hydrogen. For helium, over twice the initial operating pressure of hydrogen is

required along with significantly greater refrigeration capacity to cool to an initial temperature of 5 K.

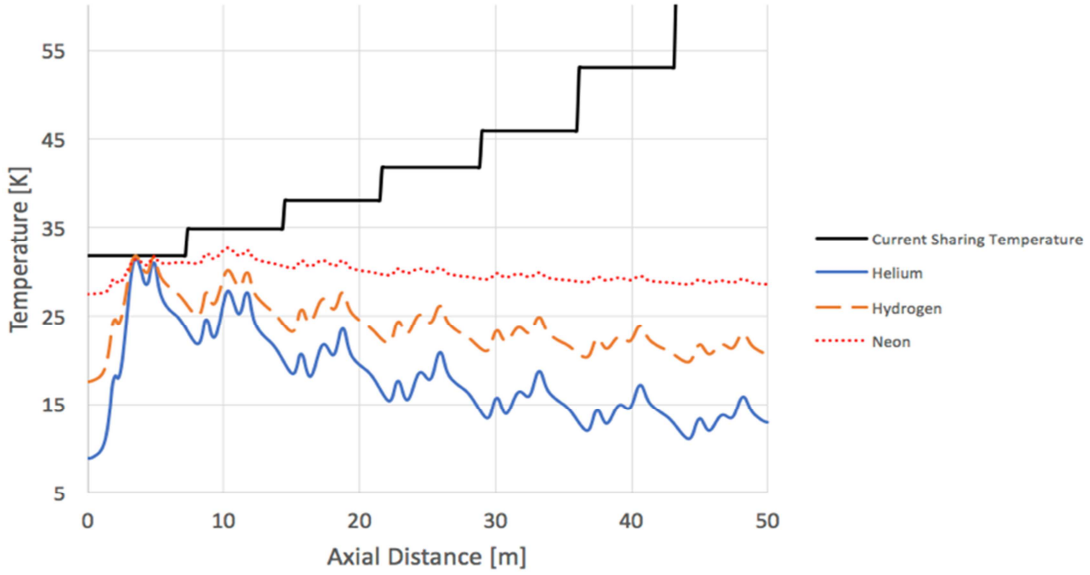


Figure 12 – Conductor temperature as a function of axial position for helium (dP = 0.0024 MPa), hydrogen (dP = 0.0025 MPa), and neon (dP = 0.0953 MPa) at the minimum flow conditions required to achieve the current sharing temperature limit. Each fluid has initial properties corresponding to Table 3.

At the initial conditions outlined in Table 3, each fluid has its strengths and weaknesses. A low pressure drop is required for helium. However, a low initial temperature of 5 K is also required to accommodate the large temperature rise of the conductor, and a high operating pressure of 3.5 MPa increases the complexity of the cryogenic system. Hydrogen has the lowest operating pressure of the three fluids, a low pressure drop, and a moderately low inlet temperature of 15 K. Although, the flammability of hydrogen presents a challenge when constructing a pressurized, forced-flow system. Neon, has the highest inlet temperature, but requires a high pressure drop and operating pressures to meet the current sharing temperature limit and ensure the fluid remains single phase throughout the cable. Table 4 summarizes the qualitative and quantitative trade-offs between the three cryogens at their optimum initial conditions.

Table 4 – Qualitative and quantitative trade-offs for helium, hydrogen, and neon at optimum operating conditions

| | Helium | Hydrogen | Neon |
|---|---|---|---|
| Pressure Drop (dP) | 0.0024 MPa | 0.0025 MPa | 0.0953 MPa |
| Operating Temperature | 5 K | 15 K | 27 K |
| Operating Pressure ($P_{inlet}$) | 3.5 MPa | 1.5 MPa | 3.0 MPa |
| Mass Flow Rate | 5.6 g/s | 4.50 g/s | 131 g/s |
| Average Flow Velocity | 0.80 m/s | 0.84 m/s | 1.42 m/s |
| Cost of Refrigerant | Moderate | Low | High |
| Flammable | No | Yes | No |

The combination of neon's high pressure drop and low temperature margins exclude it from practical implementation in the present design. With neon eliminated, helium and hydrogen can be compared to further analyze the quantitative trade-offs between both fluids.

To directly substitute helium for hydrogen, helium should match the optimum initial conditions of hydrogen (15 K/ 1.5 MPa). At these initial conditions, helium requires a pressure drop of 0.0276 MPa – over 10 times greater than hydrogen at the same conditions. The required cable pressure drop can be decreased by lowering the initial temperature and/or increasing the initial pressure of helium. However, doing so proportionally increases the required cooling capacity and complexity of the cryogenic system. To illustrate these trade-offs, Fig. 13 shows the required cable pressure drop as a function of initial temperatures, for a set of constant initial pressures.

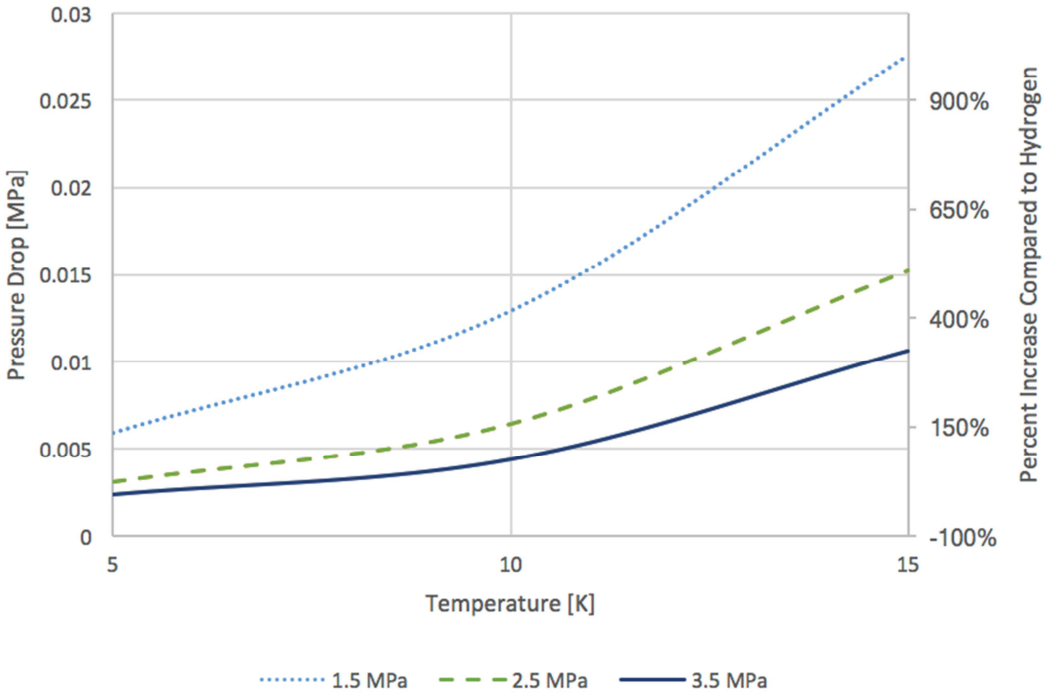


Figure 13 – Cable pressure drops for helium at various inlet temperatures and pressures compared to hydrogen at its optimal initial operating temperature and pressure (15 K/ 1.5 MPa)

With respect to the pressure drop, helium is competitive with hydrogen at low temperatures and high pressures. However, these operating conditions are not ideal. To minimize system complexity, it is beneficial to maximize initial temperature and minimize initial pressure. As shown in Fig. 13, a unit decrease in temperature for helium results in a larger reduction in dP above 10 K than below. Therefore, cooling helium below 10 K results in diminishing returns with respect to dP reduction. Moreover, as the fluid temperature decreases below 10 K, the required cooling load increases due to decreasing refrigeration efficiencies. A trend of diminishing returns can similarly be seen with respect to operating pressure. As the operating

pressure increases at constant temperature, there is a decreased reduction in dP per unit increase in pressure. Therefore, despite helium having the highest HTC at high pressures, the benefit of increasing pressure to reduce dP becomes limited. For these reasons, an operating pressure of 2.0 MPa provides helium with a balance between dP reduction and high operating pressures.

To optimize the current design across inlet temperature, cable pressure drop, and operating pressure, helium is selected to operate at 10 K and a pressure of 2.0 MPa. At these conditions, helium produces a mean HTC of 1,180 $\frac{W}{m^2K}$ with a pressure drop of 0.0088 MPa, a mass flow rate of 7.5 g/s, and a mean flow velocity of 2.38 m/s. The conductor and fluid temperatures at these helium conditions are shown in Fig. 14.

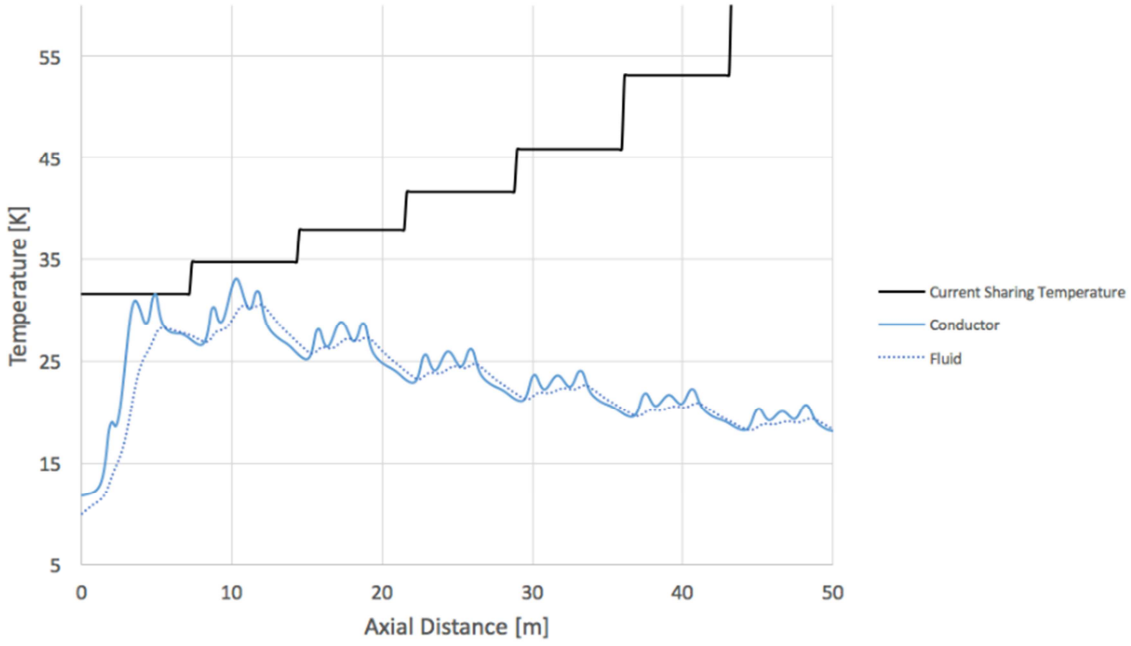


Figure 14 - Conductor and fluid temperature profiles for helium at 10 K/ 2.0 MPa

# 6.0 SUMMARY

Helium provides optimum heat transfer rates at high pressures (limited to 3.5 MPa in the current study) and low temperatures between 5-15 K. Hydrogen performs best with an initial pressure of 1.5 MPa and for temperatures in the range of 15-35 K. Finally, neon has an optimum operating pressure of 3.0 MPa and operates most effectively between 27-46 K.

To successfully cool the conductor, the temperature rise is limited by the current sharing temperature - defined by the maximum magnetic field on coil and the operating current density of the conductor. The high solidification temperature of neon (27 K) results in a high pressure drop and mass flow required to limit the temperature rise of the superconductor below the prescribed current sharing temperature limit. Neon's large pressure drop and low temperature margins excluded it from further consideration for the current design.

Helium and hydrogen were compared across three operating parameters relating to inlet temperature, cable pressure drop, and operating pressure. To directly replace hydrogen with helium at the same initial pressure and temperature, the pressure drop increased over 10 times to achieve the same current sharing condition. Optimizing the trade-offs between efficiencies, dP, and inlet temperature for helium resulted in an initial temperature and pressure of 10 K and 2.0 MPa respectively.

Hydrogen uniformly produced the highest heat transfer coefficients and overall cooling performance, making it the best cryogen for the thermal stability of the TF coil. However, the flammability of hydrogen presents regulatory and safety considerations when constructing a cryogenic system. Conversely, helium is inert and can operate over a wide range of temperatures and pressure. In scenarios where extreme neutron heat loads (> 1 $MW/m^3$) are present and temperature margins are small, the increased performance of hydrogen may necessitate its use. However, for the current design, helium is able to adequately remove the neutron heat load at operating parameters within engineering reason.

Acknowledgements:
none

Funding:
This work was supported by the U. S. DOE, Office of Fusion Energy Science
[grant number: DE-FC02-93ER54186]

# REFERENCES

[1] Whyte, D, Minervini, J, LaBombard, B, Marmar, E, Bromberg, L, & Greenwald, M 2016, 'Smaller & Sooner: Exploiting high magnetic fields from new superconductors for a more attractive fusion energy development path', *Journal Of Fusion Energy*, 35, 1, pp. 41-53

[2] LaBombard, B, et al. 2015, 'ADX: a high field, high power density, advanced divertor and RF tokamak', *Nuclear Fusion*, 55, 5, p. 053020

[3] Coppi, B, et al. 2015, 'Perspectives for the high field approach in fusion research and advances within the Ignitor Program', *Nuclear Fusion*, 55, 5, p. 053011

[4] Sorbom, B, Ball, J, Palmer, T, Mangiarotti, F, Sierchio, J, Bonoli, P, Kasten, C, Sutherland, D, Barnard, H, Haakonsen, C, Goh, J, Sung, C, & Whyte, D n.d., 'ARC: A compact, high-field, fusion nuclear science facility and demonstration power plant with demountable magnets', *Fusion Engineering And Design*, 100, pp. 378-405

[5] Brassington, D, & Cairns, D 1977, 'Measurements of forced convective heat transfer to supercritical helium', *International Journal Of Heat And Mass Transfer*, 20, 3, pp. 207-214

[6] P.J. Linstrom and W.G. Mallard, Eds., NIST Chemistry WebBook, NIST Standard Reference Database Number 69, National Institute of Standards and Technology, Gaithersburg MD, 20899

[7] Munson, B. R., D. F. Young, T. H. Okiishi, and W. W. Huebsch, *Fundamentals of Fluid Mecahnics*, 6th ed. Wiey, Hoboken, NJ, 2009.

[8] C.A. Thompson, W. M. Manganaro and F.R. Fickett 1990, Cryogenic Properties of Copper, International Copper Association, Ltd., National Institute of Standards and Technology, Boulder CO

[9] Gnielinski V. New equations for heat and mass transfer in turbulent pipe flow and channel flow. *International Chemical Engineering*, 1976; 16: 359-368.